the plant journal

SEB SOCIETY FOR EXPERIMENTAL BIOLOGY

The Plant Journal (2023) **114,** 7–22 doi: 10.1111/tpj.16149

N^6-Methyladenosine modification of mRNA contributes to the transition from 2D to 3D growth in the moss *Physcomitrium patens*

David Garcias-Morales[1], V. Miguel Palomar[2], Florence Charlot[3], Fabien Nogué[3], Alejandra A. Covarrubias[1] and José L. Reyes[1,*]

[1]*Departamento de Biología Molecular de Plantas, Instituto de Biotecnología, UNAM, Av. Universidad 2001, Cuernavaca, CP 62210, Mexico,*

[2]*Department of Molecular, Cellular and Developmental Biology, University of Michigan, 1105 N. University Ave, Ann Arbor, MI, 48109-1085, USA, and*

[3]*Université Paris-Saclay, INRAE, AgroParisTech, Institut Jean-Pierre Bourgin (IJPB), 78000, Versailles, France*

Received 12 September 2022; revised 7 February 2023; accepted 10 February 2023; published online 16 February 2023.
*For correspondence (e-mail jose.reyes@ibt.unam.mx).

SUMMARY

Plants colonized the land approximately 470 million years ago, coinciding with the development of apical cells that divide in three planes. The molecular mechanisms that underly the development of the 3D growth pattern are poorly understood, mainly because 3D growth in seed plants starts during embryo development. In contrast, the transition from 2D to 3D growth in the moss *Physcomitrium patens* has been widely studied, and it involves a large turnover of the transcriptome to allow the establishment of stage-specific transcripts that facilitate this developmental transition. N^6-Methyladenosine (m^6A) is the most abundant, dynamic and conserved internal nucleotide modification present on eukaryotic mRNA and serves as a layer of post-transcriptional regulation directly affecting several cellular processes and developmental pathways in many organisms. In Arabidopsis, m^6A has been reported to be essential for organ growth and determination, embryo development and responses to environmental signals. In this study, we identified the main genes of the m^6A methyltransferase complex (MTC), *MTA*, *MTB* and *FIP37*, in *P. patens* and demonstrate that their inactivation leads to the loss of m^6A in mRNA, a delay in the formation of gametophore buds and defects in spore development. Genome-wide analysis revealed several transcripts affected in the *Ppmta* background. We demonstrate that the *PpAPB1–PpAPB4* transcripts, encoding central factors orchestrating the transition from 2D to 3D growth in *P. patens*, are modified by m^6A, whereas in the *Ppmta* mutant the lack of the m^6A marker is associated with a corresponding decrease in transcript accumulation. Overall, we suggest that m^6A is essential to enable the proper accumulation of these and other bud-specific transcripts directing the turnover of stage-specific transcriptomes, and thus promoting the transition from protonema to gametophore buds in *P. patens*.

Keywords: MTA, MTB, FIP37, PpAPB, epitranscriptome, gametophore bud formation.

Linked article: This paper is the subject of a Research Highlight article. To view this Research Highlight article visit https://doi.org/10.1111/tpj.16173.

INTRODUCTION

One of the main characteristics that allowed plants to colonize the land 470 million years ago was the development of apical cells that divide in three planes (Graham et al., 2000). Apical cells are present in the lineage of charophycean algae from which land plants originated; nevertheless, these organisms grow only in either one or two planes, creating a net of filaments or branching mats (Niklas, 2000). Later in evolution, plant apical cells gained the ability to divide in three dimensions (3D), allowing the acquisition of a new array of shapes and the colonization of new spaces.

The molecular mechanisms that underly the development of 3D growth are poorly understood, mainly because 3D growth in seed plants starts during embryo development, and therefore mutants exhibiting defects in 3D growth are lethal (Meinke & Sussex, 1979; Sun et al., 1998). The life cycle of the moss *Physcomitrium patens*

recapitulates the transition from filamentous growth, to planar branching, to full 3D growth, and a similar transition occurs later during the development of its zygote (Cove & Knight, 1993; Govindan et al., 2022; Harrison et al., 2009). Nonetheless, mutations in genes involved in the transition from 2D to 3D growth are not lethal, as plants can survive by filamentous growth indefinitely (Moody et al., 2018), turning *P. patens* into an ideal model to study 3D growth modulation in plants.

The life cycle of *P. patens* begins with the germination of a haploid spore, from which a filamentous structure called protonema emerges, growing by uniplanar cell division. The protonema is composed of two cell types: chloronema, which has numerous chloroplasts, and caulonema, which contains oblique cell walls and fewer chloroplasts (Cove et al., 2006; Menand et al., 2007). The 2D growth form continues when the subapical cells divide, originating side branches called secondary protonema; however, some of the subapical cells can divide in a new 3D growth pattern to give rise to stem cells named gametophore buds (Aoyama et al., 2012; Cove & Knight, 1993; Harrison et al., 2009). These buds divide in three planes to first develop into gametophores, which are composed of leaf-like structures known as phyllids and root-like rhizoids. The gametophores later develop sexual organs: female archegonia and male antheridia. The diploid zygote is originated when the egg is fertilized by one flagellated sperm cell, and this zygote undergoes 3D growth to generate the sporophyte composed of foot, seta and capsule, where thousands of haploid spores are produced by meiosis to complete the life cycle (Harrison et al., 2009).

The transition from 2D to 3D growth in *P. patens* has been widely studied and a mechanism for its regulation has been proposed (Moody, 2019). The principal regulators of this transition are the PpAPB transcription factors, which are the orthologs of the Arabidopsis AINTEGUMENTA, PLETHORA and BABY BOOM proteins. These transcription factors (PpAPB1–PpAPB4) are indispensable for the formation of gametophore buds, and a quadruple mutant is incapable of forming gametophore initial cells (Aoyama et al., 2012). Transcription of the *PpAPB* genes is affected in the absence of DEFECTIVE KERNEL 1 (PpDEK1) (Demko et al., 2014; Johansen et al., 2016; Perroud et al., 2014) and NO GAMETOPHORES 1 (PpNOG1)(Moody et al., 2018). Thus, the current proposed mechanism suggests that PpDEK1, a calpain protease, represses the transcription of the *PpAPB* genes by cleaving a putative transcription activator, whereas PpNOG1 would promote their transcription by targeting a putative repressor for ubiquitination and ensuing degradation (Moody et al., 2018). More recent evidence has suggested that PpNOG1 could directly regulate the subcellular accumulation of DEK1, pointing to another path for *APB* regulation (Perroud et al., 2020). The transcription of the *PpAPB* genes is also upregulated by auxins. Once the transcription of these genes is achieved, the transition from 2D to 3D is initiated, promoting the activation of several cytokinin response regulators (Aoyama et al., 2012). However, other participants in this process remain to be discovered. In particular, the transition from 2D to 3D growth in *P. patens* has been shown to involve a large turnover of the transcriptome, and this process must be finely regulated to establish a set of stage-specific transcripts that facilitate the transition to a 3D growth pattern (Frank & Scanlon, 2015).

There are numerous post-transcriptional mechanisms known to regulate mRNA abundance, among them, the addition of N^6-methyladenosine (m^6A), an mRNA chemical modification, has recently emerged as a process to directly modulate the metabolism of the transcripts at the transcriptome level (Frye et al., 2018; Ivanova et al., 2017; Wang et al., 2021). m^6A is the most abundant and well characterized internal mRNA modification, and its transcriptome landscape is dynamically regulated by the activity of different proteins that install (m^6A methyltransferases), remove (m^6A demethylases) and recognize (m^6A-binding factors) this modification (Shi et al., 2019). The addition of the methyl group is catalyzed by a large methyltransferase complex (MTC) in which the METTL3/METTL14 (methyltransferase-like 3/14) heterodimer acts as the catalytic core, and WTAP (Wilms' tumor 1-associated protein) allows the interaction with several protein factors that modulate its activity (Garcias Morales & Reyes, 2021). In plants, the MTC has been identified and orthologs of METTL3, METTL14 and WTAP, named MTA, MTB and FIP37, respectively, have been studied, mostly in *Arabidopsis thaliana* (Bodi et al., 2012; Růžička et al., 2017; Shen et al., 2016; Zhong et al., 2008). The biological effects of m^6A modification of mRNA in plants are diverse, including the regulation of organ growth and determination (Arribas-Hernández et al., 2018; Růžička et al., 2017; Shen et al., 2016), embryo development (Zhong et al., 2008) and responses to environmental signals (Anderson et al., 2018; Govindan et al., 2022; Hu et al., 2021).

Here, we identified the gene orthologs of *MTA*, *MTB* and *FIP37* in the moss *P. patens* and demonstrate that the m^6A methyltransferase activity on mRNA is abolished in the null mutants of these genes. The absence of m^6A in mRNA leads to defects in the moss life cycle, as shown by a delay in gametophore bud formation and defects in spore development and viability. Unlike *A. thaliana*, the mutant plants of the MTC are viable and can be propagated indefinitely by protonemal growth. We demonstrate that transcripts of all four *PpAPB*s are methylated and that the absence of methylation in *Ppmta* mutant plants drives the decrease of these transcripts, resulting in a delay in the transition from 2D to 3D growth. We propose that m^6A modification of mRNA is required to facilitate the transition from 2D to 3D growth by regulating the abundance of

several mRNAs, including the *PpAPB* transcripts, encoding for the master regulators of this developmental pathway.

RESULTS AND DISCUSSION

The m^{6}A methyl transferase complex is conserved in *Physcomitrium patens*

In the genome of *P. patens*, we identified genes that have a high percentage of identity with MTC core genes previously identified in *A. thaliana*, used here as a reference. We selected *PpMTA* (Pp3c1_32590V3.1, 70% identity with Arabidopsis MTA) and *PpFIP37* (Pp3c8_10480V3.1, 69% identity with Arabidopsis FIP37), annotated as putative orthologous genes of *MTA* (Zhong et al., 2008) and *FIP37* (Shen et al., 2016). A recent report (Yue et al., 2019) where the authors used sequence information from 15 land plant species and seven algae species to identify homologs of the m^{6}A machinery confirmed that the two *P. patens* genes we selected, *PpMTA* and *PpFIP37*, are the most certain orthologs of *MTA* and *FIP37*, respectively. We generated mutant lines for these two genes using the CRISPR/Cas9 technology previously reported for *P. patens* (Lopez-Obando et al., 2016). In the recovered lines, we confirmed the presence of a mutation caused by nucleotide deletions in these loci by genomic PCR and sequencing (diagrams showing the mutations obtained are presented in Figure S1). To confirm that the subsequent results are caused by the absence of m^{6}A-MTC activity instead of potential Cas9 off-target artifacts, we generated the complemented lines PpMTA-C and PpFIP37-C. In these two lines, the mutation was replaced with the native sequence using homologous recombination. The identity of the complemented lines was confirmed by PCR and sequencing of the relevant gene region to confirm the wild-type (WT) sequence. First, we tested for the presence of a transcript in all mutant and complemented plants using reverse transcription-quantitative PCR (RT-qPCR) (Figure 1a). We observed an absence of transcript accumulation in the *Ppmta* and *Ppfip37* mutant lines when compared with the WT line (probably caused by premature stop codons present in the mutant genes, see Figure S1); by contrast, the PpMTA-C and PpFIP37-C lines showed a recovery of the corresponding transcript, similar to the accumulation detected in the WT line. To address whether the presence of m^{6}A in mRNA is affected in the mutant lines, we performed a dot-blot assay using poly-A+ RNA and incubated it with an antibody that recognizes the m^{6}A modification (Figure 1b). We observed a severe reduction of the m^{6}A signal in the *Ppmta* and *Ppfip37* mutant lines when compared with the WT sample; furthermore, the m^{6}A signal was recovered in the PpMTA-C and PpFIP37-C lines. These results confirm that *PpMTA* and *PpFIP37* are the orthologous genes of the Arabidopsis MTC components; however, in contrast with Arabidopsis, the mutant *P. patens* plants do not show a lethal phenotype during gametophytic growth and can be maintained by protonemal propagation indefinitely.

PpMTB1 and PpMTB2 are essential for m^{6}A addition to mRNA

In addition to *PpMTA* and *PpFIP37* we identified two proteins, PpMTB1 and PpMTB2 (Pp3c5_5900V3.1 and Pp3c6_26980V3.1, respectively), that share a high percentage of identity (81% and 67%, respectively) with *MTB*, the Arabidopsis ortholog of METTL14. The same genes were previously identified as potential orthologs of *MTB* (Yue et al., 2019). Nevertheless, in organisms where m^{6}A addition has been reported, the METTL14 protein, an essential factor of the MTC, is always encoded by a single gene. We generated single and double mutants for the *PpMTB1* and *PpMTB2* putative genes using CRISPR-Cas9 genome editing. We obtained mutations that resulted in the formation of a premature stop codon in the *Ppmtb1* and *Ppmtb2* single mutants (Figure S1). The accumulation of the corresponding transcripts, analyzed by RT-qPCR, showed a drastic reduction in the single mutants, probably because of the presence of the premature stop codon (Figure 1c). Then, we analyzed the presence of m^{6}A in poly-A+ RNA by performing a dot-blot assay. We observed that the single mutants displayed an m^{6}A signal similar to that of the WT plants (Figure 1d). Thus, we obtained a *Ppmtb1 Ppmtb2* double mutant line carrying the same alleles as the single mutants that showed a significant reduction in the m^{6}A signal, similar to that of the *Ppmta* mutant (Figure 1d). This result indicates that *PpMTB1* and *PpMTB2* genes are both active and could function redundantly in m^{6}A catalysis in *P. patens*, raising the possibility that the heterodimer with PpMTA within the MTC might be assembled in some cases with PpMTB1 and in other cases with PpMTB2, adding a new layer of complexity to m^{6}A catalysis in *P. patens*.

Loss of m^{6}A function causes a delay in gametophore bud development

Having established the molecular defects caused by mutations in the genes encoding for the core components of the MTC complex, we analyzed the effects of the absence of m^{6}A catalysis throughout the life cycle of *P. patens*. First, we evaluated the growth of the protonema, and to do so we obtained protoplasts from 7-day-old protonema from *Ppmta*, *Ppfip37*, a quadruple mutant (*Ppmta Ppfip37 Ppmtb1 Ppmtb2*, hereafter QM) and WT plants. After 7 days of growth on PpNH4 medium, no significant difference in plant area was observed among the mutant lines when compared with that of the WT plants (Figure S2), suggesting that at this developmental stage, the presence of m^{6}A in mRNA is not essential, allowing the protonema to be continuously propagated.

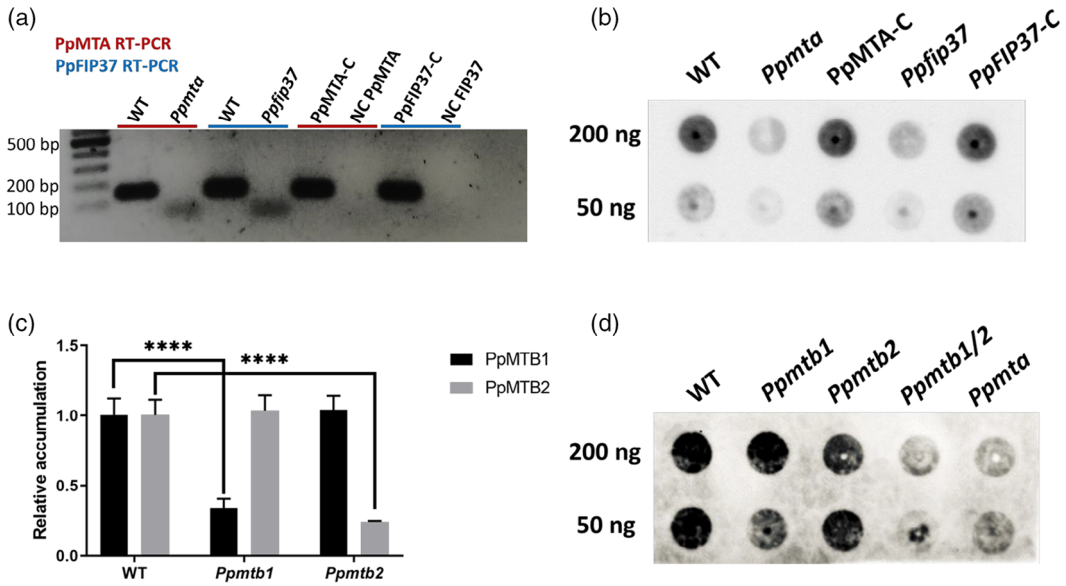

Figure 1. Mutation of the MTC genes affects the addition of N^6-methyladenosine (m^6A) to mRNA.
a Total RNA was isolated from *Ppmta*, *Ppfip37*, complemented lines (PpMTA-C and PpFIP37-C) and wild-type (WT) plants (2 weeks old), and subjected to RT-qPCR to evaluate the presence of the corresponding transcripts (*PpMTA*, indicated in red; *PpFIP37*, indicated in blue). NC MTA and NC FIP37 correspond to PCR negative control samples. (b) A dot-blot immune-assay was employed to detect N^6-methyladenosine (m^6A) levels in poly-A+ RNA isolated from WT, *Ppmta*, PpMTA-C, *Ppfip37* and PpFIP37-C plants at 2 weeks old. Two different quantities of poly-A+ RNA were used in each case (50 and 200 ng). (c) Total RNA was isolated from wild type, *Ppmtb1*,and *Ppmtb2* plants, and subjected to RT-qPCR to evaluate the abundance of the corresponding transcripts. The mRNA for *ACT7* was used as the reference gene. Statistical significance was evaluated with a Student's *t*-test (****$P < 0.001$). Error bars represent standard deviations for two independent biological samples with three technical replicates each. (d) A dot-blot immune-assay was performed to detect m^6A levels in poly-A+ RNA isolated from WT, *Ppmtb1*, *Ppmtb2*, *Ppmtb1 Ppmtb2* and *Ppmta* plants. Two different quantities of poly-A+ RNA were used for each sample (50 and 200 ng).

Next, we explored the formation of gametophore buds. For this experiment we obtained protoplasts from 7-day-old protonema from *Ppmta*, PpMTA-C, *Ppfip37*, PpFIP37-C and WT plants and after 14 days of growth the number of buds was counted and classified in three different visual categories: early buds (bulb shape), mid buds (heart shape), and late buds (first phyllid and presence of rhizoids, see Figure S3). The total number of gametophore buds and those progressing to the late developmental categories were dramatically reduced in the mutant lines (Figure 2a). These phenotypes are clearly associated with the absence of m^6A catalysis, as the complemented lines showed a number of gametophore buds with a maturity distribution similar to that of the WT plants (Figure 2a). The mutant phenotypes of reduced bud number and the reduction of late buds could be associated with lower production or, alternatively, a delay in their formation. To further dissect this phenotype, we counted the number of gametophores in 20-day-old plants and we classified them based on the number of phyllids they bore. The *Ppmta* and *Ppfip37* mutant lines showed a reduced number of gametophores with a smaller number of phyllids in comparison with PpMTA-C, PpFIP37-C and the WT plants, which had gametophores that bore up to eight phyllids (Figure 2b,c). Importantly, bud development continued over time in all genetic backgrounds, as evidenced by the number of resulting gametophores in 20-day-old plants (compare the number of buds in Figure 2a with the number of gametophores in Figure 2b). However, the mutant lines displayed buds and gametophores mainly at younger developmental stages. Together, these results indicate that the reduced number of buds and gametophores observed in the mutant lines is not caused by an arrest in their growth, but instead is consistent with a delay in developmental progression, and that this phenotype is dependent on m^6A catalysis.

These features were also evaluated in the *Ppmtb1*, *Ppmtb2* and *Ppmtb1 Ppmtb2* lines. In this case we did not observe any obvious defect in the *Ppmtb1* and *Ppmtb2* single mutant lines. Nevertheless, the *Ppmtb1 Ppmtb2* double mutant displayed a decrease in the number and maturity of buds and gametophores comparable with those obtained with the *Ppmta* mutant (Figure 2d–f). These results indicate that *PpMTB1* and *PpMTB2* are necessary for correct bud and gametophore formation. Moreover, this requirement, together with the reduced m^6A level in mRNA observed only in the double mutant (see Figure 1d), suggests that *PpMTB1* and *PpMTB2* act redundantly, at least during these developmental stages.

So far, we have identified the main components of the MTC described in other species. The mutants of the *PpMTA*, *PpFIP37*, *PpMTB1* and *PpMTB2* genes show reduced levels of m^6A modification on mRNA and similar phenotypic defects during bud and gametophore

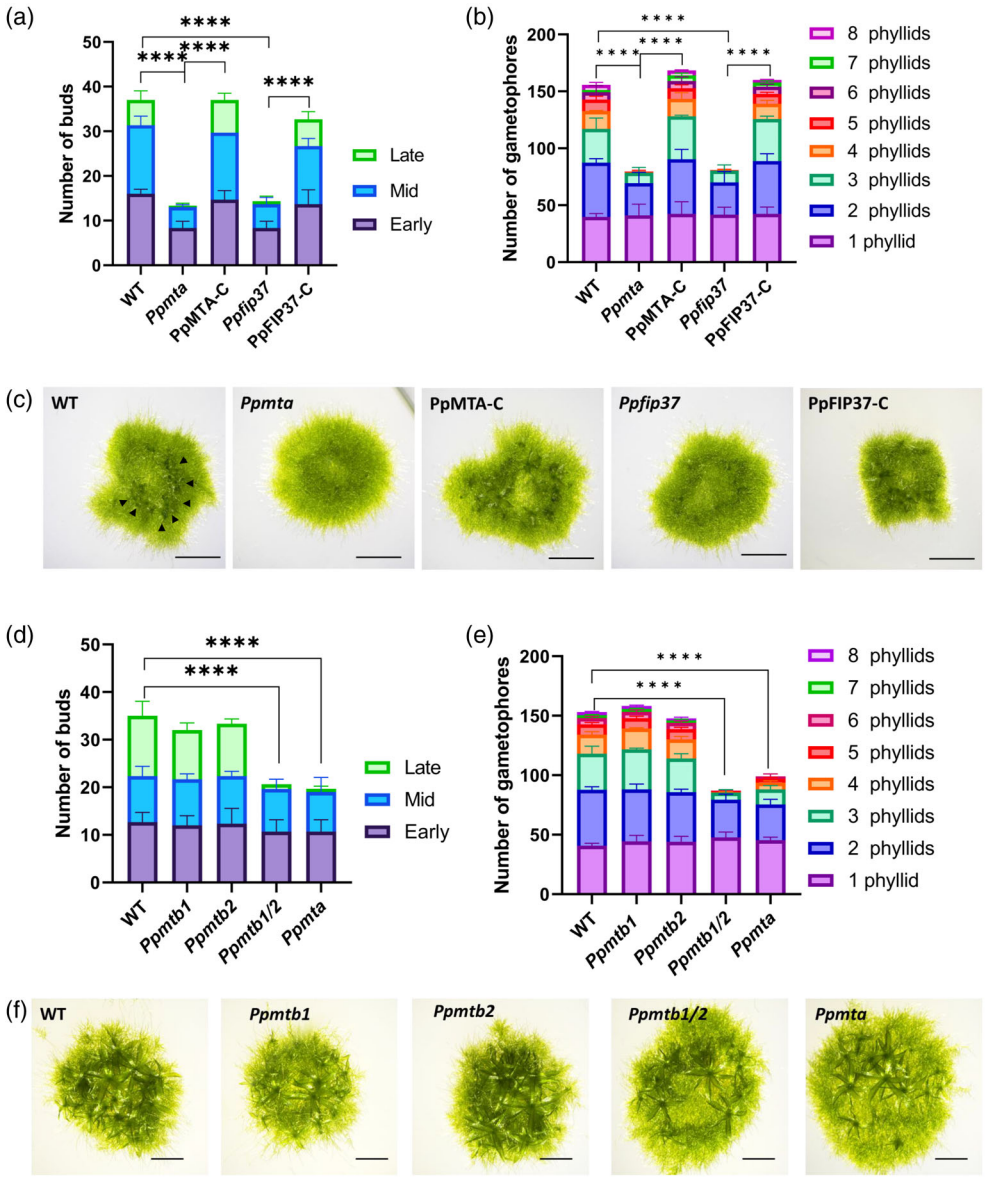

Figure 2. Mutants of the methyltransferase complex (MTC) genes show a delay in the development of gametophore buds.
a Fourteen-day-old plants were dissected to visualize gametophore buds that were visually classified into three different stages of growth (early, mid and late). Five plants of each genotype, wild type (WT), *Ppmta*, PpMTA-C, *Ppfip37* and PpFIP37-C, were counted for each of three independent biological replicates. Statistical significance was evaluated using analysis of variance (ANOVA) (****$P < 0.001$). Error bars represent standard deviations. (b) Twenty-day-old plants were dissected to visualize gametophores that were classified according to the number of phyllids they bore. Five plants of each genotype (WT, *Ppmta*, PpMTA-C, *Ppfip37* and PpFIP37-C) were counted for each of three independent biological replicates. Statistical significance was evaluated using ANOVA (****$P < 0.001$). Error bars represent standard deviation. (c) Individual plants from the different genotypes evaluated in (b), as seen under the stereoscope. Black arrowheads indicate the presence of gametophores in WT plants as a reference. Scale bars: 5 mm. (d) Fourteen-day-old plants were dissected to visualize gametophore buds that were classified into three different stages of growth (early, mid and late). Five plants of each genotype (wild type, *Ppmtb1*, *Ppmtb2*, *Ppmtb1 Ppmtb2* and *Ppmta*) were counted for each of three independent biological replicates. Statistical significance was evaluated using ANOVA (****$P < 0.001$). Error bars represent standard deviations. © Twenty-day-old plants were dissected to visualize gametophores that were classified according to the number of phyllids they bore. Five plants of each genotype (WT, *Ppmtb1*, *Ppmtb2*, *Ppmtb1 Ppmtb2* and *Ppmta*) were counted for each of three independent biological replicates. Statistical significance was evaluated using ANOVA (****$P < 0.001$). Error bars represent standard deviations. (f) Individual plants from the different genotypes (WT, *Ppmtb1*, *Ppmtb2*, *Ppmtb1 Ppmtb2* and *Ppmta*) analyzed in © were grown for another 10 days (to 1 month of age) and viewed under the stereoscope to better show the gametophores. Scale bars: 5 mm.

development, suggesting that they are involved in the regulation of the transition from protonema to gametophore bud formation. Consistently, when we evaluated the expression of the MTC core genes in a previous RNA-seq analysis of bud cells and protonemal apical cells collected separately by laser microdissection (Frank & Scanlon, 2015), we observed that the *PpMTA*, *PpFIP37*, *PpMTB1* and *PpMTB2* transcripts showed an abundant

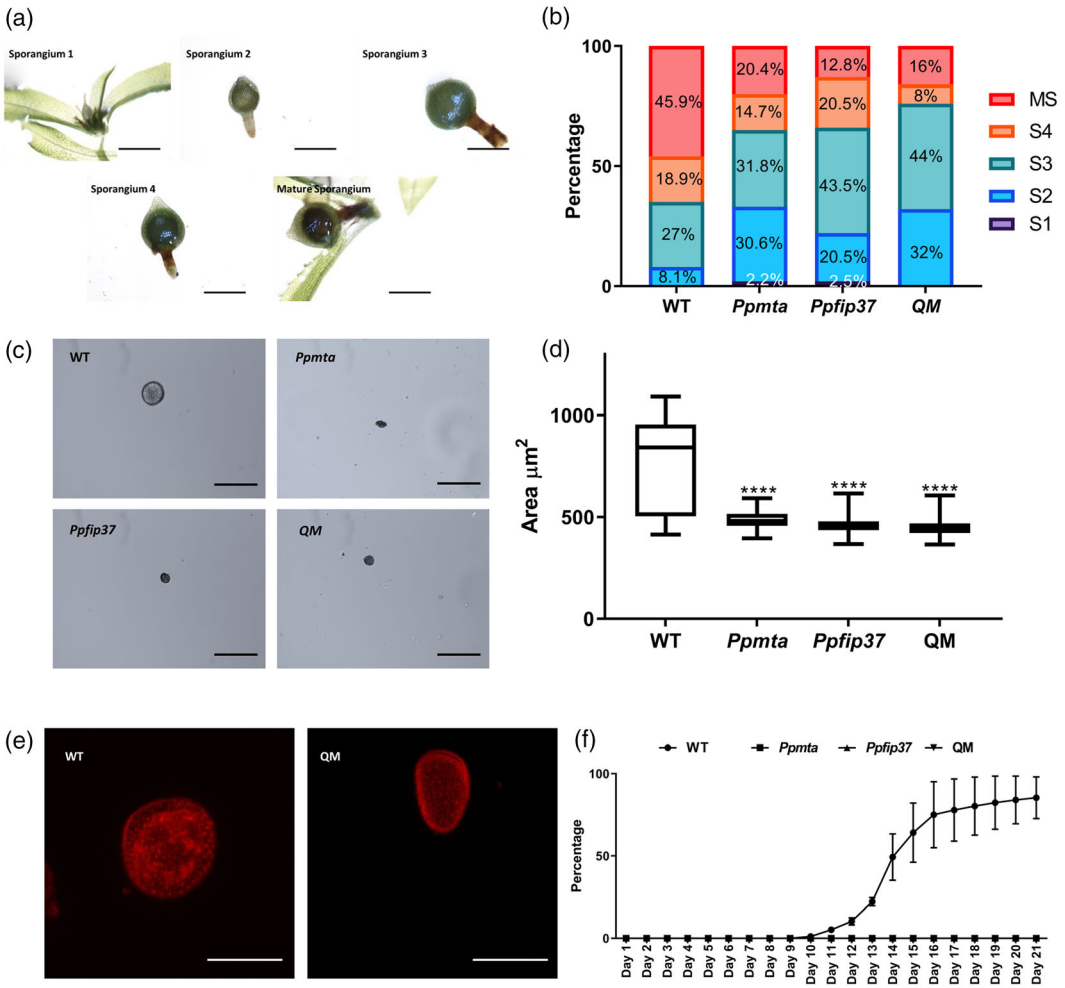

Figure 3. Disruption of N^6-methyladenosine (m^6A) addition triggers aberrant spore phenotypes.
a Sporangia were observed under a stereoscope and the different growth stages were visually classified into five categories: stages 1–4 (S1–S4) and mature sporangia (MS). Scale bars: 500 mm. (b) Sporangia were counted from wild type (WT), *Ppmta*, *Ppfip37* and QM (*Ppmta Ppfip37 Ppmtb1 Ppmtb2*) plants, classified according to the different growth stages as S1–S4 or MS, and represented as percentages of the total. Between 144 and 163 sporangia were collected from all the plants grown in three magenta boxes per each of three independent experiments. (c) Spores from mature sporangia (MS) from each genotype analyzed in (b) were photographed to calculate the area. Scale bars: 25 µm. A total of 150 spores were collected in each of three independent experiments. (d) Measurement of spore area for each genotype as indicated. Statistical significance was evaluated using ANOVA (****$P < 0.001$). © Representative spores from WT and QM plants were observed using multiphotonic confocal microscopy. Scale bars: 25 mm. (f) Mature spores from WT, *Ppmta*, *Ppfip37* and QM plants were tested for germination efficiency in PpNH4 medium supplemented with 10 mM $CaCl_2$ and incubated for as long as indicated in the figure. Germination of at least 250 spores was counted for each of three technical replicates of three independent biological experiments. Error bars represent standard deviations.

accumulation specifically in bud cells (see Table S1 in Frank & Scanlon, 2015), correlating with the contribution of the m^6A modification of mRNA to gametophore bud formation.

The development and viability of spores is affected in the MTC mutant plants

To extend the phenotypic analysis throughout the life cycle of *P. patens* and uncover other effects caused by the absence of m^6A catalysis, we evaluated the development of the spores and their viability. To this end, we examined *Ppmta*, *Ppfip37*, QM and WT plants. For this experiment, we considered the delay previously observed in the development of buds in the mutants, to let the plants grow for 8 weeks instead of 6 weeks under standard conditions (25°C, with 16 h light/8 h dark), allowing the different plant lines to produce as many gametophores as possible, before the induction of gametangia development (15°C, with 8 h light/16 h dark). We collected all the sporangia 4 weeks post-induction and classified them into different maturation stages according to their morphological features (e.g. size, shape and color; Figure 3a). All mutant lines showed a lower percentage of mature sporangia (12–20%) than that of the WT plants (46%) (Figure 3b), indicating that m^6A modification of mRNA participates in sporangium development in *P. patens*. Considering that the

publicly available expression data sets indicate that the major accumulation of the transcripts encoding for the MTC proteins occurs during the development of the sporophyte, and specifically in the mature spore (Figure S4; eFP Browser, http://bar.utoronto.ca/efp_physcomitrella/cgi-bin/efpWeb.cgi), we focused on the morphology and viability of the spores. We evaluated the spores obtained only from mature sporangia and analyzed their size, morphology and viability. The spores of all the mutant lines tested exhibited a strong reduction in their size (Figure 3c,d) and an abnormal shape, with a flattened shape that is completely different in morphology from the regular round shape observed in the WT spores (Figure 3e). Lastly, we evaluated the germination rate of the spores isolated from *Ppmta*, *Ppfip37*, QM and WT plants. We observed that the spores of all mutant lines were unable to germinate, whereas the spores of WT plants reached the highest percentage of germination at 10 days (Figure 3f). These results reveal that the components of the MTC are also required for the proper development and germination of the spores; consequently, MTC absence leads to a lethal phenotype preventing the life cycle of *P. patens* to be completed. This phenotype resembles that of the embryonic lethality observed in Arabidopsis *mta* and *fip37* mutants, in which the mutant embryos exhibit a developmental arrest during the globular stage, where normally the embryo undergoes asymmetrical cell divisions leading to the establishment of the 3D pattern (Shen et al., 2016; Zhong et al., 2008). The molecular mechanisms governing zygote development in the life cycle of *P. patens* are not understood. Although there are clear differences between the 3D growth of the sporophyte and the 3D growth occurring during gametophore bud formation, it remains unknown whether these two processes share similar factors, in part because most of the mutants affected in 3D growth patterning do not form gametophores and in consequence the development of the sporophyte cannot be analyzed (Aoyama et al., 2012; Moody et al., 2018; Perroud et al., 2014). Future work in *P. patens* will help uncover the role of MTC factors in these developmental steps.

Identification of m^{6}A-modified mRNAs revealed that all *PpAPB* transcripts are methylated

Here, we demonstrate that the m^{6}A pathway plays a relevant role in the development of the spores and their germination; however, because of the lack of information on the molecular pathways underlying this process, we decided to first evaluate the molecular contribution of the m^{6}A mRNA modification to the metabolism of the transcripts during the transition from protonema to gametophore bud development. For this, we identified the m^{6}A-modified transcripts using 18-day-old WT plants treated with naphthalene acetic acid (NAA) and kinetin, to increase the number of buds and therefore magnify the signal originating from the bud-specific transcriptome. As the methylated RNA immunoprecipitation sequencing (MeRIP-seq) analysis has not been employed before in *P. patens* plants at this growth stage, we first tested the suitability of the m^{6}A antibody. For this purpose, we performed an m^{6}A-immunoprecipitation assay and analyzed the accumulation of some transcripts by RT-PCR in the different fractions obtained: initial poly-A+ RNA (input), immunoprecipitated fraction (m^{6}A) and unbound fraction (non-m^{6}A). To investigate whether some of the mRNAs encoding for factors involved in bud development are modified by m^{6}A, we selected a potential ortholog of the mitogen-activated protein kinase kinase *YODA* mRNA, which is methylated in Arabidopsis (Shen et al., 2016) and is highly accumulated in bud cells (Frank & Scanlon, 2015). We also included *DEK1* and *PpAPB1*, which are central factors in the developmental pathway of gametophore buds, and as negative controls we selected *UBI10* and *ACT7* because no methylation of these mRNAs has been described. From this analysis we observed that *PpAPB1* and *PpYDA*, the putative ortholog of *YODA*, were enriched in the m^{6}A fraction, whereas *ACT7*, *UBI10* and *DEK1* were mainly enriched in the non-m^{6}A fraction (Figure 4a), demonstrating that the antibody has the specificity required to discriminate among transcripts, and indicating its selectivity to immunoprecipitate m^{6}A-modified mRNAs. Consequently, we performed an MeRIP-seq analysis to identify methylated mRNAs at the transcriptome level. We identified 2532 methylation peaks spread over 2270 transcripts, indicating that some of these have more than one methylation peak (Table S2). The m^{6}A peaks were enriched near the stop codon and, to a lesser extent, towards the start codon (Figure 4b), an observation that has also been reported in other plant species (Luo et al., 2014; Xu et al., 2021). By applying MEME algorithms to identify potential methylation sequence motifs enriched in these regions, we found a 7-nt sequence with the consensus GRAGRAG (where R = A/G, P = 9.1e-056; Figure 4c). Previous reports have shown that in plants the methylation motif RRACH has undergone diversification, and furthermore, depending on the tissue, growth conditions or environmental stimuli, the modified mRNAs exhibit different consensus motifs (Anderson et al., 2018; Govindan et al., 2022; Zhou et al., 2022). Here, we propose GRAGRAG as a methylation motif present in *P. patens* during bud formation; however, it is necessary to carry out additional tests to confirm the functionality of this motif and define which adenosine is being methylated within this consensus sequence.

Next, we performed a Gene Ontology (GO) analysis of the 2270 transcripts identified by MeRIP-seq, revealing an enrichment of several RNA metabolism-related categories, although no obvious association with bud development was recognized (Figure S5). Importantly, we found that *PpAPB1* and *PpAPB2* mRNAs are present in our MeRIP-seq

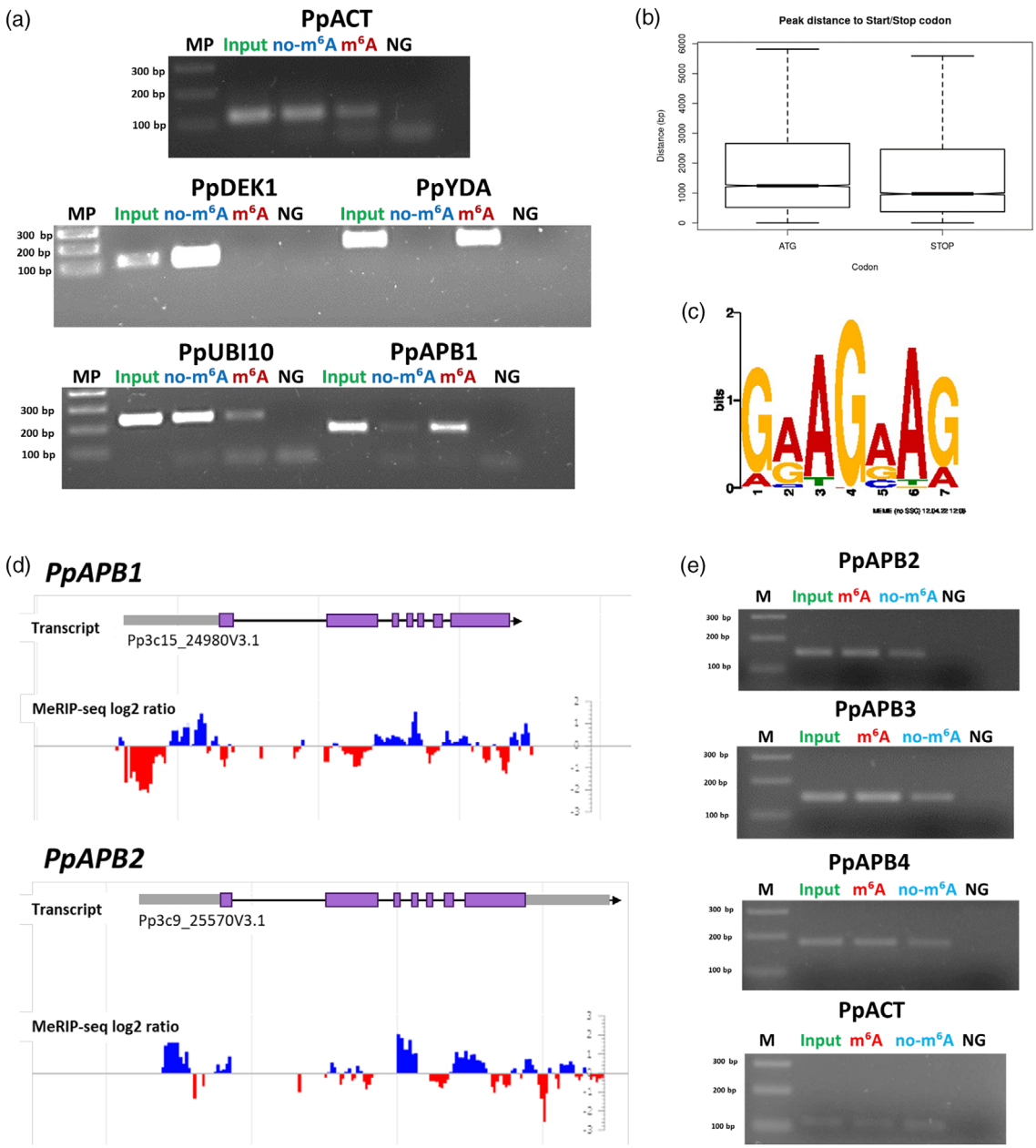

Figure 4. The transcripts of *PpAPB*s are methylated and detected by MeRIP-seq in bud-enriched plants.
a Poly-A+ RNA was isolated from 18-day-old wild type plants treated with naphthalene acetic acid (NAA, 1 μM) for 5 days and then kinetin (1 μM) for 1 day. A fraction of the recovered RNA was saved (input, shown in green) and the remaining was used for immunoprecipitation using the anti-m^{6}A antibody (m^{6}A fraction, shown in red); the unbound fraction was also recovered (no-m^{6}A, in blue). The three fractions were subjected to RT-qPCR to evaluate the presence of different transcripts, as indicated. NG: negative control of PCR reaction. (b) Distance distribution of m^{6}A-containing peaks identified by MeRIP-seq, towards start or stop codons. (c) The MEME suite of algorithms was used to identify potential conserved motifs in the 2270 peaks obtained from the MeRIP-seq analysis, returning the 7-nt-long motif GRAGRAG (R = A/G, *P* = 9.1e-056). (d) Diagrams show the gene structure for *PpAPB1* (Pp3c15_24980v3.1) and *PpAPB2* (Pp3c9_25570v3.1). The plots below indicate the position of enriched peaks shown as the log^2 ratio of immunoprecipitation/input (in blue and red bars). © Poly-A+ RNA from wild-type plants was used for m^{6}A-immunoprecipitation. A fraction of the starting RNA sample was saved (input, shown in green) and the remaining was used for immunoprecipitation using the anti-m^{6}A antibody (m^{6}A fraction, shown in red); the unbound fraction was also recovered (no-m^{6}A, in blue). The fractions obtained were subjected to RT-qPCR to evaluate the presence of *PpAPB2*–*PpAPB4* and *ACT5* transcripts, as indicated. NG: negative control of PCR reaction.

analysis (Figure 4d). As a result of this finding, we examined whether *PpAPB3* and *PpAPB4* mRNAs are also methylated. To do so, we performed an m^{6}A-immunoprecipitation RT-qPCR assay and confirmed that *PpAPB2*, *PpAPB3* and *PpAPB4* mRNAs are enriched in the m^{6}A fraction, indicating that all four *PpAPB* transcripts can be modified by m^{6}A (Figure 4a,e). In contrast to *PpAPB1* and *PpAPB2*, the mRNAs for *PpAPB3*, *PpAPB4* and *PpYDA*, the putative

ortholog of *YODA*, which we detected in our m^{6}A-IP-RT-PCR, were not found in the MeRIP-seq analysis as high-confidence candidates. This result could be explained by the fact that we did not specifically employ tissues originating from bud cells, and the m^{6}A signal from the bud-specific transcripts could have been diluted. Alternatively, the MeRIP-seq assay may underestimate the abundance of m^{6}A-modified mRNAs with low expression levels (Dominissini et al., 2013; Shen et al., 2016), and thus other important m^{6}A-modified transcripts may remain to be discovered. Nonetheless, the presence of m^{6}A in all four *PpAPB* mRNAs could affect their metabolism and, in consequence, contribute to gametophore bud development and be consistent with the phenotype observed in the MTC mutants during the developmental transition from protonema to gametophore buds. To investigate the relationship between the presence of m^{6}A in mRNA and its accumulation, we analyzed the molecular defects caused by its absence in the *Ppmta* mutant.

The metabolism of several m^{6}A-modified mRNAs is affected in the *Ppmta* mutant

To further examine the global effect of the addition of m^{6}A on mRNA in the *P. patens* transcriptome during the transition from protonema to gametophore buds, we performed an RNA-seq analysis to compare the *Ppmta* mutant and the WT transcriptomes. To this end, we employed 18-day-old plants of both genotypes treated with NAA and kinetin, to increase bud formation, as described before. We identified 1081 differentially expressed (DE) transcripts, including 520 downregulated and 561 upregulated genes (Figure S6; Table S3). When we searched for enriched GO categories using these DE transcripts, we did not detect any that were directly related to gametophore bud development, and mostly detected GO categories associated with metabolic processes, probably as a consequence of developmental activity (Figure S6). Next, to investigate the direct effect of m^{6}A modification on gene expression during this developmental stage, we compared the results of the RNA-seq and MeRIP-seq analyses, where we identified 79 DE mRNAs that were also modified by m^{6}A (Figure 5a; Table S4). We first arranged these 79 recovered transcripts according to their differential expression, from up- to downregulated (33 and 46 mRNAs, respectively). When we observed the extent of methylation in each mRNA (as defined by the *P*-value), there was no clear association between this value and the direction of changes in mRNA accumulation (Figure 5a), suggesting that additional factors determine the fate of the m^{6}A-containing transcripts to direct them to down- or upregulation, as described in other biological systems (Frye et al., 2018; Ivanova et al., 2017; Wang et al., 2021), including plants (Anderson et al., 2018; Govindan et al., 2022). Among these 79 m^{6}A-DE transcripts we identified factors involved in the development of buds, for instance *PpAPB2* (Pp3c9_25570) (Aoyama et al., 2012), and others related to auxin signaling, such as the ARF domain protein (Pp3c6_21370V3.1) and the AUX/IAA domain factor (Pp3c15_9710V3.1), which are methylated and downregulated in *Ppmta* plants (indicated by aqua asterisks in Figure 5a,c; Figure S7). Furthermore, we performed a GO analysis using only these 79 m^{6}A-DE transcripts, where we identified processes related to the development of gametophore buds, including categories such as shoot system development, multicellular organism development and postembryonic development (indicated by purple asterisks in Figure 5b). Among the mRNAs included in these categories, we recognized the presence of SNF1 Kinase Interactor-like protein (Pp3c16_25700), Epidermal Patterning Factor-like protein (Pp3c23_5720), Inosine-Uridine Preferring Nucleoside Hydrolase (Pp3c26_14640) and UDP-glucuronate 4-epimerase (Pp3c11_14370) (indicated by red asterisks in Figure 5a; Figure S7). However, their participation during bud development has not been studied, and therefore their analysis can add new clues and enlighten the molecular mechanisms underlying the transition from protonema to gametophore buds, through the regulation of their mRNA metabolism resulting from the addition of m^{6}A.

Loss of m^{6}A affects the stability of *PpAPB* transcripts

As shown above, we identified *PpAPB2* as an m^{6}A-DE mRNA, and the loss of m^{6}A is associated with a decrease in its accumulation in *Ppmta* plants (Figure 5a). Moreover, we showed that all *PpAPB* transcripts are methylated (Figure 4a,e), and thus we analyzed the mRNA accumulation of *PpAPB1*, *PpAPB3* and *PpAPB4* in the *Ppmta* plants. The RNA-seq analysis showed that they tend to be downregulated in the mutant plants (Figure 5c), suggesting that m^{6}A is important to allow the appropriate accumulation levels of these transcripts. However, it is necessary to directly test whether this reduction is caused by the absence of m^{6}A. In this respect, one of the principal mechanisms that m^{6}A employs to facilitate the turnover of the transcriptome is by offering stability to transcripts that are important for the establishment of the new cellular stage. To assess this possibility, we employed actinomycin D to inhibit global transcription in *Ppmta* and WT plants and measured the mRNA accumulation levels of *PpAPB*s over time (at 0, 2, 4, 6 and 12 h). Accordingly, in WT plants all transcripts showed a reduction in their abundance over time, consistent with mRNA turnover. However, all four *PpAPB*s showed a larger decrease in their mRNA levels in *Ppmta* plants, when compared with the levels observed in WT plants, whereas no difference was observed in a non-methylated transcript (*DEK1*) (Figure 6). This result indicates that the presence of m^{6}A on *PpAPB* transcripts facilitates their correct accumulation during gametophore bud development and the absence of this modification leads to

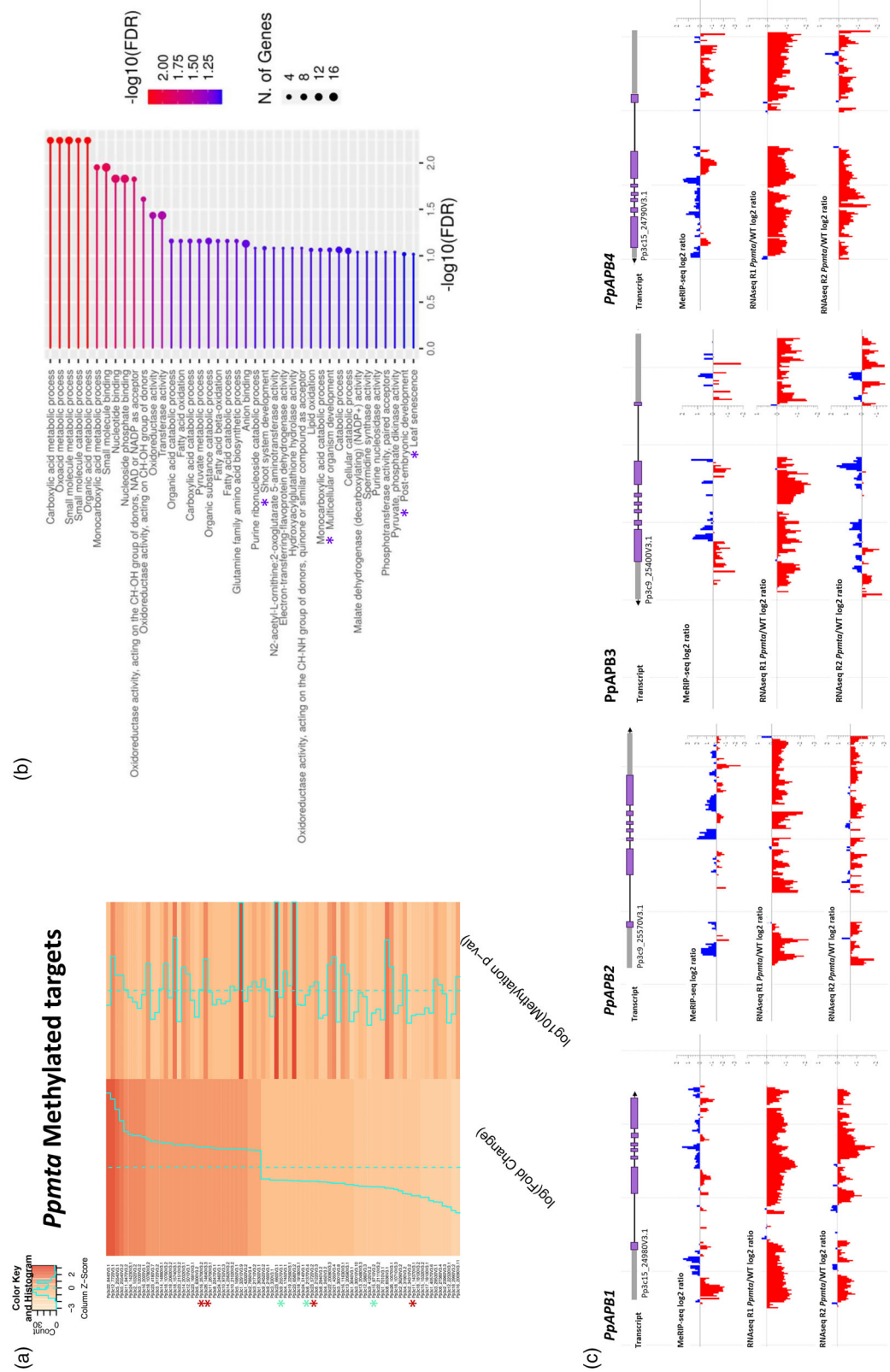

Figure 5. N^6-Methyladenosine (m^6A)-modified transcripts show differential expression.
a Heat map of the comparison of RNA-seq analysis of *Ppmta* and wild-type (WT) plants, and MeRIP-seq of poly-A+ RNA of WT plants showing transcripts according to their differential expression, from up- to down-regulation (left column with $\log^{10}$ fold change indicated), and their corresponding methylation extent (as defined by the *P*-value). Dotted lines in aqua indicate the average value of the data and solid lines show the value for individual genes, as shown in the color and histogram key above. Genes related to bud development are indicated by aqua asterisks. Genes corresponding to GO terms highlighted in (b) are indicated by red asterisks. (b) GO analysis of the 79 differentially expressed genes obtained in (a), revealing functional categories. Categories related to developmental processes are indicated by purple asterisks. The size of the dots indicates the number of genes included in each category. Colors represent the $-\log^{10}$ value for false discovery rate (FDR). (c) Diagrams show the gene structure for *PpAPB1* (Pp3c15_24980v3.1), *PpAPB2* (Pp3c9_25570v3.1), *PpAPB3* (Pp3c9_25400v3.1) and *PpAPB4* (Pp3c15_24790v3.1). The plots below indicate the position of m^6A-enriched peaks found by MeRip-seq shown as the $\log^2$ ratio of immunoprecipitation/input (in blue and red bars). The accumulation levels obtained in the RNA-seq replicates 1 and 2 are indicated below as $\log^2$ ratio of *Ppmta*/WT, shown as blue bars (upregulated) or red bars (downregulated).

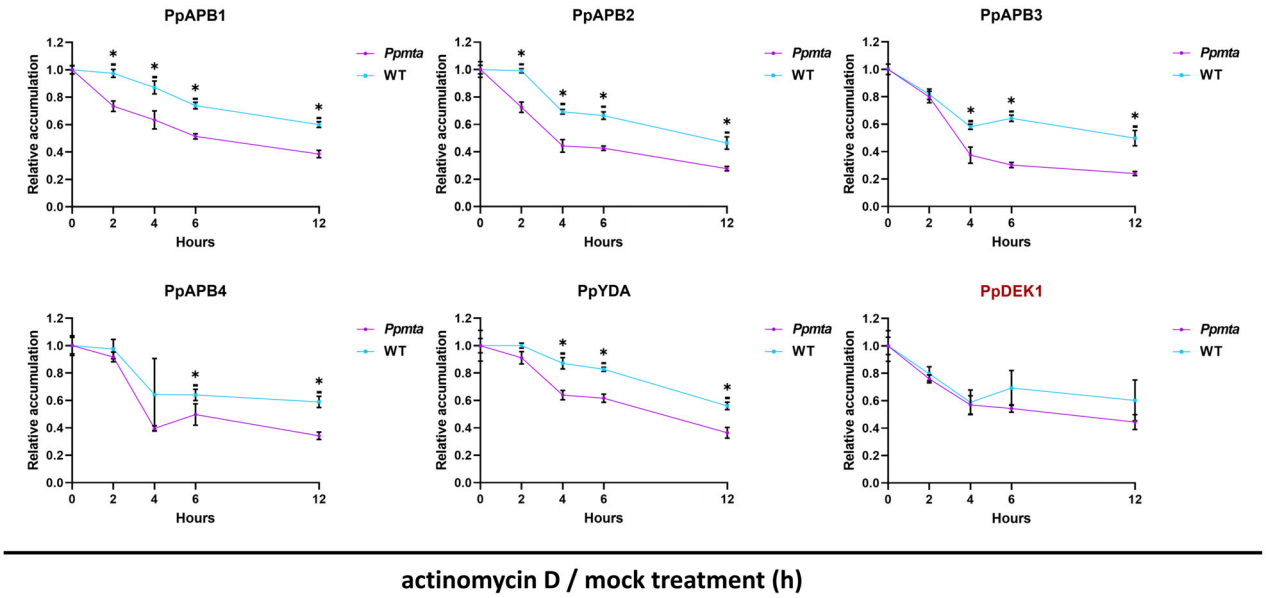

Figure 6. *N*^{6}-Methyladenosine (m^{6}A) modification confers stability to *PpABP1–PpABP4* transcripts.
Eighteen-day-old plants (*Ppmta* and wild type) were treated with naphthalene acetic acid (NAA, 1 μM) for 5 days and then kinetin (1 μM) for 1 day. After this period, plants were further divided into two groups, one treated with actinomycin D (Act10 μM) and another with mock treatment (DMSO) for 0, 2, 4, 6 or 12 h. Total RNA was isolated from these plants and subjected to RT-qPCR to evaluate the presence of transcripts encoding for *PpAPB1–PpAPB4*, the *PpYDA* putative ortholog, and *PpDEK1*. Results are shown as the value from the actinomycin D samples normalized to mock samples and referenced to the 0 h time point. Error bars represent standard deviations; *$P = 0.05$ (Student's *t*-test). The analysis was made with two independent biological samples with three technical replicates each.

a decrease in their abundance, contributing to the phenotype of delay in bud formation observed for the *Ppmta*, *Ppfip37* and *Ppmtb1 Ppmtb2* mutants (see Figure 2). Despite the contribution of m^{6}A to the stability of *PpAPB* transcripts, it is likely that other factors equally regulated by this modification contribute to the phenotype observed, such as *PpYDA*, the putative ortholog of *YODA* (Figures 4a and 6), which acts downstream of the *PpAPB*s, offering a bird's eye view of the dynamic and complex regulation mechanism mediated by this mRNA modification.

CONCLUSION

This study reports on the functions of the m^{6}A modification on mRNA in a non-vascular plant model, where we identified the main factors of the methyltransferase complex in *P. patens*. In contrast with other organisms, we identified two functional homologs for MTB, raising the possibility that different MTC complexes are formed to regulate specific substrates in the moss *P. patens*. We demonstrate that the function of the MTC is conserved and that its inactivation by mutation, and therefore the loss of the regulation mediated by m^{6}A, leads to a delay in the development of gametophore buds and more importantly yields non-viable spores. Both phenotypes resemble those observed in Arabidopsis, where the mutants of the MTC show embryos that fail to divide in three dimensions, leading to a lethal phenotype. Furthermore, we identified mRNAs that are methylated during bud development and confirmed that the *PpAPB1–PpAPB4* transcripts contain m^{6}A and that this modification facilitates their correct accumulation through the regulation of their mRNA stability. In a broader context, we propose that m^{6}A is essential to enable the appropriate levels of these and other bud-specific transcripts directing the turnover of stage-specific transcriptomes, and thus promoting the transition from protonema to gametophore buds (Figure 7a). In the MTC mutants, certain bud-specific transcripts are devoid of the regulation mediated by m^{6}A, thus failing to reach proper RNA levels, causing a delay in gametophore bud development (Figure 7b). The innovation of 3D growth in the development of plants coincides with a series of other novelties in their evolution, such as the origin of extracellular matrices (sporopollenin, cellulose, lignin and pectin, among other compounds), the establishment of intercellular communication networks (plasmodesmata and phytohormone signaling) and the diversification of gene regulatory networks to promote cell differentiation (Bowman et al., 2007; Wickett et al., 2014), suggesting that m^{6}A gained prominence in the regulation of other aspects of plant development requiring a transcriptome turnover. These features were acquired early in the evolution of plants and are conserved in flowering plants, opening new avenues to better understand how the m^{6}A modification of mRNA contributes to the evolution and regulation of 3D

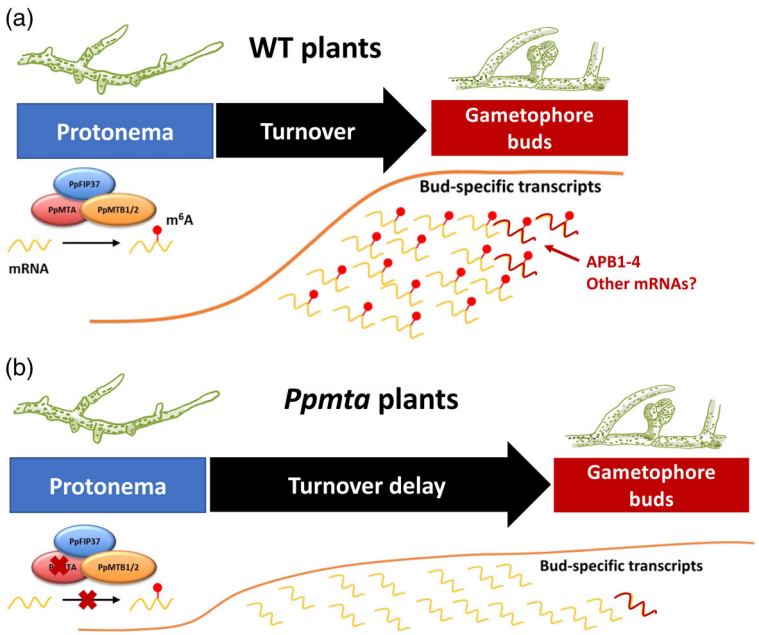

Figure 7. N^6-Methyladenosine (m^6A) modification facilitates the accumulation of bud-specific transcripts to allow the transcriptome turnover required for the transition from 2D to 3D.
Working model for the contribution of the m^6A modification of mRNA in transcripts during transcriptome reshaping to facilitate the establishment of gametophore buds from protonema. (a) In wild-type plants, the addition of m^6A to mRNAs (shown as red circles) is performed by the methyltransferase complex (MTC), consisting of PpMTA, PpFIP37 and either PpMTB1 or PpMTB2. The presence of m^6A is correlated with the increased stability and ensuing accumulation of certain transcripts, including *PpAPB1*–*PpAPB4* and probably other unidentified factors, as shown in the figure. The correct accumulation of stage-specific transcripts secures timely bud development. (b) In contrast, in the *Ppmta* mutant line the absence of MTA (or other components in individual mutants) disrupts the addition of m^6A, leading to an impaired accumulation of certain transcripts known to be involved in the development of gametophore buds (such as *PpAPB1*–*PpAPB4*) and, in consequence, a delay during this transition is observed.

growth patterning and other important processes in plant development.

EXPERIMENTAL PROCEDURES

Cloning and purification of single guide RNA (sgRNA) plasmids

Coding sequences for the *PpMTA*, *PpFIP37*, *PpMTB1* and *PpMTB2* genes were used to search for CRISPR RNA (crRNA), preceded by a protospacer adjacent motif (PAM) motif of the *Streptococcus pyogenes* Cas9 (NGG or NAG) using the webtool CRISPOR 1 (http://crispor.tefor.net/crispor.py) and the *P. patens* genome v3.3 (https://phytozome-next.jgi.doe.gov/info/Ppatens_v3_3). We selected crRNAs near the translation start codon with a high specificity score.

Moss culture and protoplast transformation

The Gransden WT strain of *P. patens* was used for this study. The moss was cultured on PpNH4 medium (Charlot et al., 2022), propagated in Percival growth chambers (Geneva Scientific, https://www.geneva-scientific.com) set to 25°C and 60% humidity with a 16-h light/8-h dark photoperiod (white light, 80 μmol m^{-2} sec^{-1}). Protoplast isolation was performed following a previously described protocol (Charlot et al., 2022). Protoplasts were incubated with 10 μg of pAct-Cas9 plasmid (Lopez-Obando et al., 2016) containing the coding sequence for the protein Cas9 and with 10–12 μg of the sgRNA plasmid for the single mutants or a mix of 10–12 μg of sgRNA plasmids for the multiple mutants. The quantity of each sgRNA plasmid in the mix was obtained by dividing the total weight of sgRNA plasmids (10–12 μg) by the number of sgRNA plasmids used for each transformation, as described previously (Lopez-Obando et al., 2016). The protoplasts were regenerated on PpNH4 medium supplemented with 0.33 M mannitol for 1 week, and then the plants on cellophane disks were transferred to PpNH4 medium supplemented with 50 μg L^{-1} of G418 for plasmid selection. The transfected plants were placed on a new PpNH4 plate without selection and were isolated after 1 week.

Genotyping using PCR screening

After 1 month of growth, individual plants were used for DNA extraction. The tissue was frozen in liquid nitrogen and ground to a fine powder. DNA extraction was performed using 2× CTAB buffer (2% acetyl-trimethylammonium bromide, 1% polyvinyl pyrrolidone, 100 mM Tris-HCl, pH 8.0, 1.4 M NaCl, 20 mM EDTA). For each sample, 500 μL of 2× CTAB extraction buffer were used, samples were mixed and transferred to a 60°C thermoblock for 30 min, then the samples were centrifuged at 14 000 × ***g*** for 5 min; the supernatant was transferred to a new tube, an equal volume of chloroform was added and mixed, and after 5 min of centrifugation at 14 000 × ***g*** the phases were separated. The aqueous upper phase was transferred to a new tube and the DNA was precipitated by adding 0.7 volumes of cold isopropanol and centrifuged at 14 000 × ***g*** for 10 min. The supernatant was discarded, and precipitated DNA was rinsed by adding 500 μL of 75% ethanol and centrifuged for 5 min at 14 000 × ***g***. The recovered genomic DNA was dissolved in 50 μL of water. To identify CRISPR/Cas9-generated mutations, the primers used for the PCR were designed to surround the target sequence and to amplify fragments of 150–200 bp (Table S1). The PCR reactions (50 μL) were performed using 1 μL of DNA sample as the template. The resulting DNA fragments were evaluated by 3% agarose TAE gel electrophoresis and when a change in size was observed, the fragment was sequenced (Unidad de Síntesis y Secuenciación de DNA, Ibt UNAM, https://ibt.unam.mx).

Generation of complemented lines

Using WT plant DNA as a template, a 2000-bp fragment of the *PpMTA* and *PpFIP37* genes was amplified by PCR (Table S1). These 2000-bp fragments contain the native sequence in the central position, with 1000 bp on each side, to restore the mutation present in *Ppmta* and *Ppfip37* mutant lines. Also, we added a *de*

novo restriction site in these fragments using the PCR overlap extension technique, to distinguish the WT plant from the complemented plant. The substitutions generate a silent mutation to preserve the original WT amino acid sequence. For the 2000-bp fragments of *PpMTA* and *PpFIP37*, new *Sac*I and *Sal*I restriction sites were generated, respectively. These fragments were cloned into pJET2.1 (ThermoFisher Scientific, https://www.thermofisher.com) and sequenced to confirm their integrity. The resulting constructs were linearized and transfected as previously described into protoplasts isolated from *Ppmta* and *Ppfip37* single mutant plants to induce homologous recombination. The resulting complemented plants were analyzed by PCR and confirmed by DNA sequencing.

Molecular characterization of transgenic lines

Total RNA was isolated from plants of different ages, as described in the text. We used the Rneasy Plant Mini kit (QIAGEN, https://www.qiagen.com) and treated the recovered RNA with Dnasel (ThermoFisher Scientific). cDNA was synthesized from 250 ng of Dnase-treated RNA using RevertAid Reverse Transcriptase (ThermoFisher Scientific). The PCR reactions (20 μL) were performed using 1 μL of cDNA template. The primers used for PCR were designed to amplify fragments of 150–200 bp (Table S1).

Dot-blot experiments to immunodetect m^{6}A were performed using polyA+ RNA extracted with oligo-dT Dynabeads (Dynabeads mRNA direct purification kit; ThermoFisher Scientific), as described by the provider. For each sample, 50 ng and 200 ng were used. The RNA samples (5 μL) were denatured by adding 1.6 μL of 4× RNA denaturing buffer (16.4 M formamide, 2.8 M formaldehyde, 26.6 m M MOPS buffer (6.7 m M sodium acetate), 1.3 m M EDTA) and incubated at 65°C for 5 min, cooled on ice, and 6.6 μL of 20× SSC buffer (3.0 M NaCl, 0.3 M sodium citrate, pH 7.0) and 6.7 μL of nuclease-free water, were added. Samples were spotted on a Hybond-N+ membrane (Amersham, now GE Healthcare, https://www.gehealthcare.com), previously placed in a 96-well dot-blot apparatus (Schleicher & Schuell BioScience). Vacuum pressure was applied to draw the solution through the membrane. After air-drying for 5 min, the membrane was crosslinked twice using the auto-crosslink setting in the apparatus (Stratalinker® UV crosslinker 1800; Stratagene, now Agilent, https://www.agilent.com) and incubated with blocking buffer (5% low-fat milk in PBS, 0.1% Tween 20 (PBS-T)) for 1 h at room temperature (24–25°C), and then incubated with N6-mA antibody (1:1000, cat. no. 56593S; Cell Signaling Technology, https://www.cellsignal.com) at 4°C overnight. Membranes were washed with PBS-T three times and then incubated with HRP-linked secondary anti-rabbit IgG antibody (1:5000; Invitrogen, now ThermoFisher Scientific) for 1 h at room temperature. After three washes with PBS-T, the membrane signal was detected with SuperSignal West Dura Extended Duration Substrate kit (ThermoFisher Scientific) and a ChemiDoc Imaging System (Bio-Rad, https://www.bio-rad.com).

Anatomical analyses

Assay of protonema growth

Protonema from the *Ppmta*, *Ppfip37* and WT plants was processed to obtain protoplasts with 3 mL of 2% driselase (D9515-25G; Sigma-Aldrich, https://www.sigmaaldrich.com) and 9 mL of 8% D-mannitol solution for 1 h. The protoplasts were filtered and centrifuged for 5 min at 250 × ***g***, and then washed three times with 10 mL of 8% D-mannitol solution. These protoplasts were counted and resuspended in liquid plating media at 10 000 protoplasts mL^{-1}, and 100 μL of this solution was plated on cellophane over solid PpNH4 medium supplemented with 0.33 M mannitol. These protoplasts grew for 4 days at 25°C with a 16-h light/8-h dark photoperiod (white light, 80 μmol m^{-2} sec^{-1}) before the plants were transferred to PpNH4 media and grown for 7 days. The protonema of all lines was imaged using an SZX7-Zoom stereoscope (Olympus, https://www.olympus-lifescience.com) at 10× magnification to detect chlorophyl autofluorescence. At least 30 plants per line were imaged, growth analysis was measured using IMAGEJ and the MORPHOLOGYMACROPUBLIC 2.6 command (Bibeau & Vidali, 2014), yielding results for area and solidity (area/convex hull area). This experiment was repeated independently three times, with 10–15 plants for each of three technical replicates.

Bud and gametophore count

We used 14-day-old plants of the *Ppmta*, *Ppfip37*, *Ppmtb1*, *Ppmtb2*, *Ppmtb1/2* and WT lines to obtain individual plants from protoplasts. We collected five clones of each line to analyze them individually using a Leica DMRA2 microscope (Leica Microsystems, https://www.leica-microsystems.com) at 40× in bright field, the buds were counted and classified in three different visual categories: early buds (bulb shape), mid buds (heart shape) and late buds (first phyllid and presence of rhizoids). This experiment was repeated independently three times.

The number of gametophores per colony was also counted in the different genetic backgrounds, we used 20-day-old plants for this analysis, and gametophores were classified according to the number of phyllids they bore. For this experiment we used five colonies per line and each colony was dissected under an Olympus SZX7-Zoom stereoscope. This experiment consisted of three independent biological replicates.

Spore generation and germination

To induce sporulation, 7-day-old protonema tissue was homogenized using a FastPrep®-24 apparatus (MP-Biomedicals, https://www.mpbio.com) and grown in peat moss substrate (Jiffy-7; Jiffy, https://jiffygroup.com), in Magenta™ boxes filled up with 150 mL of water, under sterile conditions. These plants were maintained for 8 weeks at 25°C with a 16-h light/8-h dark photoperiod, and then changed to 15°C with a 8-h light/16-h dark photoperiod for 4 weeks. Sporophytes were harvested under an Olympus SZX7-Zoom stereoscope, and we calculated the percentage of sporangia at different developmental stages (designated as S1, S2, S3, S4 and MS; for further details, see legend for Figure 3b).

Germination assays were performed using spores from at least three age-matched sporangia from the mature developmental stage (MS). Mature sporangia were bleached in 1 mL of 25% bleach for 10 min and then washed three times in 1 mL of sterile water for 10 min each time, under sterile conditions. The sporophytes were then crushed in 500 μL of sterile water to release the spores, and 100 μL of this spore suspension were diluted in 900 μL of sterile water to plate 1 mL of spore solution per Petri dish. Spores were plated on cellophane overlaid with PpNH4 medium, supplemented with 10 mM $CaCl_2$. Plates were air-dried in a laminar flow hood, sealed with micropore tape, and held at 22°C with a 16-h light/8-h dark photoperiod. Spore germination was counted daily using an Olympus SZX7-Zoom stereoscope. A spore was defined as having germinated as soon as the first deformation of the spore coat by the emerging protonemal apical filament was observed. Two or three technical replicates were performed for each of three independent biological replicates. Data were expressed as percentage germination: (germinated spores/total spores counted) × 100.

M^{6}A-immunoprecipitation RT-qPCR

To enhance the yield of mRNA recovered from buds, we implemented the protocol of Johri & Desai (1973) that uses NAA and kinetin (Sigma-Aldrich) treatment to induce approximately 12 times more buds compared with untreated plants. Wild-type plants regenerated from protoplasts were grown in PpNH4 medium for 10 days under normal conditions and then transferred to PpNH4 supplemented with 1 μg mL^{-1} of NAA and grown for 5 days, then the plants were transferred to PpNH4 supplemented with 1 μg mL^{-1} of kinetin for 1 day under normal conditions. To collect tissue, excess moisture was first removed with a sterile paper towel and then the tissue was homogenized to a fine powder using a mortar and pestle cooled with liquid nitrogen. The mRNA was isolated using the Dynabeads mRNA direct purification kit, as described by the provider. The m^{6}A-IP assay was performed as previously described (Dominissini et al., 2013), with minor modifications. Briefly, we used 5 μg of mRNA (isolated as previously described) to perform an m^{6}A-immunoprecipitation using an m^{6}A-specific antibody (Cell Signaling Technology, https://www.cellsignal.com). For the m^{6}A-immunoprecipitation RT-qPCR assays, we performed the RNA immunoprecipitation without fragmenting the mRNA. We obtained the immunoprecipitated fraction (m^{6}A fraction) as well as the unbound fraction (non-m^{6}A fraction). These fractions plus the input mRNA were reverse transcribed using Revertaid reverse transcriptase (ThermoFisher Scientific) with dT primer, and different transcripts were analyzed by semi-quantitative PCR.

MeRIP-seq

Approximately 5 μg of mRNA was extracted using the Dynabeads mRNA direct purification kit (ThermoFisher Scientific) from plants that were under NAA and kinetin treatment, as previously described. The mRNA was treated with the fragmentation buffer (10 mM Tris-HCl, pH 7.0, 10 mM $ZnCl_2$) to obtain approximately 200 nt fragments. An aliquot of fragmented RNA was saved as input control, and the remainder was incubated with m^{6}A antibody (ab151230; Abcam, https://www.abcam.com), in 1× IP buffer (0.2 M Tris-HCl, pH 7.4, 1 M NaCl, 2% IGEPAL CA630) supplemented with RiboLock Rnase Inhibitor (ThermoFisher Scientific) overnight at 4°C. The antibody-bound RNA was then incubated with pre-blocked protein-A magnetic beads (Invitrogen, now ThermoFisher Scientific) at 4°C for 2 h with constant rotation. The immunoprecipitated RNA was released using an elution buffer (1× IP buffer supplemented with 6.7 mM N^6-methyladenosine; Sigma-Aldrich) and purified using ethanol precipitation. The resulting RNA samples were subjected to high-throughput sequencing in an Illumina NextSeq 500 sequencer (Illumina, https://www.illumina.com) at the Unidad Universitaria de Secuenciación Masiva y Bioinformática, IBT-UNAM. Low-quality reads and adapters were removed from >13 million total reads per sample using TRIM_GALORE 0.4.1. Mapping to the *P. Patens* genome v3.3 available at Phytozome (https://phytozome.jgi.doe.gov) was performed using BOWTIE 2.2.9 (Langmead & Salzberg, 2012), allowing a single mismatch (mapping rate > 76%). Reads were PCR de-duplicated using Picard tools. Narrow peak calling was performed using MACS 2.1.1.20160309 (Zhang et al., 2008) with a haploid genome length of 475 Mbp, and only peaks with $P < 0.05$ were kept. The full peak sequence was used for *de novo* motif discovery using MEME-SUITE 5.4.1 (Bailey et al., 2015). The raw next-generation sequencing (NGS) data reported in this work has been deposited to the National Center for Biotechnology Information (NCBI) database as series GSE213348.

RNA-seq

Protonemal tissue from WT and *Ppmta* plants that were subjected to NAA and kinetin treatment (as described above) was collected to isolate total RNA using the Rneasy Plant Mini Kit (QIAGEN) and the integrity of the RNA was measured with a Bioanalyzer 2100 (Agilent, https://www.agilent.com). cDNA libraries were obtained using the True-Seq stranded mRNA Library Prep kit (Illumina) and sequenced using a NextSeq 500 platform (Illumina) with a configuration of 2 × 75 paired-end sequences (Unidad Universitaria de Secuenciación Masiva y Bioinformática, IBT-UNAM). Low-quality reads were removed as mentioned above from at least 30 million total reads per library and mapped to the *P. patens* genome v3.3 available at Phytozome with at least 72% mapping efficiency. Differential expression analysis was carried out using EDGER (Robinson et al., 2010), and only genes that showed a significant change ($P < 0.001$, logFC > 0.5, FDR < 0.01) were retained for downstream analysis. We carried out a GO enrichment analysis using ShinyGO with default settings (Ge et al., 2020). Correspondence between MeRIPseq and RNAseq analyses was performed using BEDTOOLS 2.25.0. To test for the significance of the set of 79 genes that showed an overlap between RNA-seq and MeRIP-seq, we used the set of 2270 genes showing m^{6}A methylation and obtained 1000 sets of 1000 randomly selected genes, to estimate the probability of overlap by chance. On average, this test returned 36 genes (P = 3.4e-06 using a Student's *t*-test). The raw NGS data reported in this work have been deposited in the NCBI database as series GSE213348.

mRNA stability assay

Protonemal tissue from WT and *Ppmta* plants was subjected to NAA treatment for 4 days (as previously stated). After 1 day on PpNH4 medium supplemented with 1 μg mL^{-1} kinetin, the plants were transferred to PpNH4 medium containing 10 μM actinomycin D or DMSO (mock treatment). Total RNA was extracted from tissue collected after 0, 2, 4, 6 and 12 h of treatment using the QIAGEN Rneasy Plant Mini Kit (QIAGEN) and subjected to Dnase I digestion. After cDNA synthesis, the accumulation of different transcripts was examined by RT-qPCR using the gene-specific primers listed in Table S1.

ACKNOWLEDGMENTS

DGM was supported by a scholarship (817571) from Consejo Nacional de Ciencia y Tecnología, México. We acknowledge the work of Selene Fernández from LANGEBIO-IPN for the initial analysis of the MeRIP-seq data. We also thank Ma. Beatríz Pérez Morales for her excellent technical support during the development of this work. This work was partially supported by grants from DGAPA-PAPIIT (IN-208421) and CONACyT (FC-2015-184) to JLR. The IJPB benefits from the support of Saclay Plant Sciences-SPS (ANR-17-EUR-0007).

AUTHOR CONTRIBUTIONS

DGM performed the experiments, analyzed the data and wrote the first draft of the article. FC and FN generated mutant lines. VMP performed the bioinformatic analyses. AAC contributed to data analysis, discussion, and article preparation. FN and JLR conceived this project, JLR supervised the project, analyzed the data and coordinated the manuscript preparation. All authors contributed to writing the article and approved the final version for publication.

CONFLICT OF INTEREST

The authors declare that they have no conflicts of interest associated with this work.

DATA AVAILABILITY STATEMENT

The raw NGS data reported in this work have been deposited to the NCBI database as series GSE213348.

SUPPORTING INFORMATION

Additional Supporting Information may be found in the online version of this article.

Figure S1. CRISPR/Cas9 editing of MTC genes causes frameshift mutations.

Figure S2. Early protonema growth is not affected in the MTC mutant lines.

Figure S3. Classification of gametophore buds according to developmental stages.

Figure S4. The accumulation of methyltransferase complex transcripts is larger during sporophyte development.

Figure S5. Gene Ontology categories of m^{6}A modified transcripts recovered by MeRIP-seq analysis.

Figure S6. Analysis of RNA-seq data obtained from *Ppmta* and wild-type plants.

Figure S7. Selected transcripts showing m^{6}A presence and the corresponding differential accumulation in *Ppmta* and wild-type plants.

Table S1. List of oligonucleotides used in this work.

Table S2. m^{6}A peaks identified in mRNA by MeRIP-seq analysis.

Table S3. Differential expression analysis of RNA-seq performed with WT and *Ppmta* mutant plants during gametophore bud formation.

Table S4. List of the 79 differentially expressed mRNAs that were also m^{6}A-modified according to MeRIP-seq.

REFERENCES

Anderson, S.J., Kramer, M.C., Gosai, S.J., Yu, X., Vandivier, L.E., Nelson, A.D.L. et al. (2018) N6-Methyladenosine inhibits local Ribonucleolytic cleavage to stabilize mRNAs in Arabidopsis. *Cell Reports*, **25**, 1146–1157.

Aoyama, T., Hiwatashi, Y., Shigyo, M., Kofuji, R., Kubo, M., Ito, M. et al. (2012) AP2-type transcription factors determine stem cell identity in the moss Physcomitrella patens. *Development*, **139**, 3120–3129.

Arribas-Hernández, L., Bressendorff, S., Hansen, M.H., Poulsen, C., Erdmann, S. & Brodersen, P. (2018) An m ^{6} A-YTH module controls developmental timing and morphogenesis in Arabidopsis. *Plant Cell*, **30**, 952–967.

Bailey, T.L., Johnson, J., Grant, C.E. & Noble, W.S. (2015) The MEME suite. *Nucleic Acids Research*, **43**, W39–W49.

Bibeau, J.P. & Vidali, L. (2014) Morphological Analysis of Cell Growth Mutants in Physcomitrella. In: Žárský, V. & Cvrčková, F. (Eds.) *Plant Cell Morphogenesis. Methods in Molecular Biology*. Totowa, NJ: Humana Press, pp. 201–213. Available from: https://doi.org/10.1007/978-1-62703-643-6_17

Bodi, Z., Zhong, S., Mehra, S., Song, J., Graham, N., Li, H. et al. (2012) Adenosine methylation in Arabidopsis mRNA is associated with the 3′ end and reduced levels cause developmental defects. *Frontiers in Plant Science*, **3**, 48.

Bowman, J.L., Floyd, S.K. & Sakakibara, K. (2007) Green genes—comparative genomics of the green branch of life. *Cell*, **129**, 229–234.

Charlot, F., Goudounet, G., Nogué, F. & Perroud, P.-F. (2022) Physcomitrium patens Protoplasting and Protoplast Transfection. In: Wang, K. & Zhang, F. (Eds.) *Protoplast Technology. Methods in Molecular Biology*. New York, NY: Springer US, pp. 3–19. Available from: https://doi.org/10.1007/978-1-0716-2164-6_1

Cove, D., Bezanilla, M., Harries, P. & Quatrano, R. (2006) Mosses as model systems for the study of metabolism and development. *Annual Review of Plant Biology*, **57**, 497–520.

Cove, D.J. & Knight, C.D. (1993) The Moss Physcomitrella patens, a model system with potential for the study of plant reproduction. *Plant Cell*, **5**, 1483–1488.

Demko, V., Perroud, P.-F., Johansen, W., Delwiche, C.F., Cooper, E.D., Remme, P. et al. (2014) Genetic analysis of *DEFECTIVE KERNEL1* loop function in three-dimensional body patterning in *Physcomitrella patens*. *Plant Physiology*, **166**, 903–919.

Dominissini, D., Moshitch-Moshkovitz, S., Salmon-Divon, M., Amariglio, N. & Rechavi, G. (2013) Transcriptome-wide mapping of N6-methyladenosine by m6A-seq based on immunocapturing and massively parallel sequencing. *Nature Protocols*, **8**, 176–189.

Frank, M.H. & Scanlon, M.J. (2015) Cell-specific transcriptomic analyses of three-dimensional shoot development in the moss Physcomitrella patens. *Plant Journal*, **83**, 743–751.

Frye, M., Harada, B.T., Behm, M. & He, C. (2018) RNA modifications modulate gene expression during development. *Science*, **361**, 1346–1349.

Garcias Morales, D. & Reyes, J.L. (2021) A birds'-eye view of the activity and specificity of the mRNA m ^{6} A methyltransferase complex. *WIREs RNA*, **12**, E1618. Available from: https://doi.org/10.1002/wrna.1618

Ge, S.X., Jung, D. & Yao, R. (2020) ShinyGO: a graphical gene-set enrichment tool for animals and plants. *Bioinformatics*, **36**, 2628–2629.

Govindan, G., Sharma, B., Li, Y., Armstrong, C.D., Merum, P., Rohila, J.S. et al. (2022) mRNA N ^{6} -methyladenosine is critical for cold tolerance in Arabidopsis. *Plant Journal*, **111**(4), 1052–1068. Available from: https://10.1111/tpj.15872

Graham, L.E., Cook, M.E. & Busse, J.S. (2000) The origin of plants: body plan changes contributing to a major evolutionary radiation. *Proceedings of the National Academy of Sciences of the United States of America*, **97**, 4535–4540.

Harrison, C.J., Roeder, A.H.K., Meyerowitz, E.M. & Langdale, J.A. (2009) Local cues and asymmetric cell divisions underpin body plan transitions in the Moss Physcomitrella patens. *Current Biology*, **19**, 461–471.

Hu, J., Cai, J., Park, S.J., Lee, K., Li, Y., Chen, Y. et al. (2021) *N* ^{6} -Methyladenosine mRNA methylation is important for salt stress tolerance in *Arabidopsis*. *The Plant Journal*, **106**, 1759–1775.

Ivanova, I., Much, C., Di Giacomo, M. et al. (2017) The RNA m 6 a reader YTHDF2 is essential for the post-transcriptional regulation of the maternal transcriptome and oocyte competence. *Molecular Cell*, **67**, 1059–1067.e4.

Johansen, W., Ako, A.E., Demko, V., Perroud, P.-F., Rensing, S.A., Mekhlif, A.K. et al. (2016) The DEK1 calpain linker functions in three-dimensional body patterning in Physcomitrella patens. *Plant Physiology*, **172**, 1089–1104.

Johri, M.M. & Desai, S. (1973) Auxin regulation of Caulonema formation in Moss Protonema. *Nature New Biology*, **245**, 223–224.

Langmead, B. & Salzberg, S.L. (2012) Fast gapped-read alignment with bowtie 2. *Nature Methods*, **9**, 357–359.

Lopez-Obando, M., Hoffmann, B., Géry, C., Guyon-Debast, A., Téoulé, E., Rameau, C. et al. (2016) Simple and efficient targeting of multiple genes through CRISPR-Cas9 in Physcomitrella patens. *G3 GenesGenomesGenetics*, **6**, 3647–3653.

Luo, G.-Z., MacQueen, A., Zheng, G., Duan, H., Dore, L.C., Lu, Z. et al. (2014) Unique features of the m6A methylome in Arabidopsis thaliana. *Nature Communications*, **5**, 5630.

Meinke, D.W. & Sussex, I.M. (1979) Embryo-lethal mutants of Arabidopsis thaliana: a model system for genetic analysis of plant embryo development. *Developmental Biology*, **72**, 50–61.

Menand, B., Calder, G. & Dolan, L. (2007) Both chloronemal and caulonemal cells expand by tip growth in the moss Physcomitrella patens. *Journal of Experimental Botany*, **58**, 1843–1849.

Moody, L.A. (2019) The 2D to 3D growth transition in the moss Physcomitrella patens. *Current Opinion in Plant Biology*, **47**, 88–95.

Moody, L.A., Kelly, S., Rabbinowitsch, E. & Langdale, J.A. (2018) Genetic regulation of the 2D to 3D growth transition in the Moss Physcomitrella patens. *Current Biology*, **28**, 473–478.e5.

Niklas, K.J. (2000) The evolution of plant body plans—a biomechanical perspective. *Annals of Botany*, **85**, 411–438.

Perroud, P., Demko, V., Johansen, W., Wilson, R.C., Olsen, O. & Quatrano, R.S. (2014) Defective Kernel 1 (DEK 1) is required for three-dimensional growth in *P hyscomitrella patens*. *The New Phytologist*, **203**, 794–804.

Perroud, P.-F., Meyberg, R., Demko, V., Quatrano, R.S., Olsen, O.-A. & Rensing, S.A. (2020) DEK1 displays a strong subcellular polarity during Physcomitrella patens 3D growth. *The New Phytologist*, **226**, 1029–1041.

Robinson, M.D., McCarthy, D.J. & Smyth, G.K. (2010) edgeR: a Bioconductor package for differential expression analysis of digital gene expression data. *Bioinformatics*, **26**, 139–140.

Růžička, K., Zhang, M., Campilho, A., Bodi, Z., Kashif, M., Saleh, M. et al. (2017) Identification of factors required for m6A mRNA methylation in Arabidopsis reveals a role for the conserved E3 ubiquitin ligase HAKAI. *The New Phytologist*, **215**, 157–172.

Shen, L., Liang, Z., Gu, X., Chen, Y., Teo, Z.W.N., Hou, X. et al. (2016) N 6 -Methyladenosine RNA modification regulates shoot stem cell fate in Arabidopsis. *Developmental Cell*, **38**, 186–200.

Shi, H., Wei, J. & He, C. (2019) Where, when, and how: context-dependent functions of RNA methylation writers, readers, and erasers. *Molecular Cell*, **74**, 640–650.

Sun, J.G., Yao, X.L., Yang, Z.X. & Zhu, Z.P. (1998) An Arabidopsis embryonic lethal mutant with reduced expression of alanyl-tRNA synthetase gene. *Cell Research*, **8**, 119–134.

Wang, Y.-J., Yang, B., Lai, Q., Shi, J.F., Peng, J.Y., Zhang, Y. et al. (2021) Reprogramming of m6A epitranscriptome is crucial for shaping of transcriptome and proteome in response to hypoxia. *RNA Biology*, **18**, 131–143.

Wickett, N.J., Mirarab, S., Nguyen, N., Warnow, T., Carpenter, E., Matasci, N. et al. (2014) Phylotranscriptomic analysis of the origin and early diversification of land plants. *Proceedings of the National Academy of Sciences of the United States of America*, **111**, E4859–E4868.

Xu, Z., Shi, X., Bao, M., Song, X., Zhang, Y., Wang, H. et al. (2021) Transcriptome-wide analysis of RNA m6A methylation and gene expression changes among two Arabidopsis ecotypes and their reciprocal hybrids. *Frontiers in Plant Science*, **12**, 685189. Available from: https://doi.org/10.3389/fpls.2021.685189

Yue, H., Nie, X., Yan, Z. & Weining, S. (2019) N6-methyladenosine regulatory machinery in plants: composition, function and evolution. *Plant Biotechnology Journal*, **17**, 1194–1208.

Zhang, Y., Liu, T., Meyer, C.A., Eeckhoute, J., Johnson, D.S., Bernstein, B.E. et al. (2008) Model-based analysis of ChIP-Seq (MACS). *Genome Biology*, **9**, R137.

Zhong, S., Li, H., Bodi, Z., Button, J., Vespa, L., Herzog, M. et al. (2008) MTA is an Arabidopsis messenger RNA adenosine Methylase and interacts with a homolog of a sex-specific splicing factor. *Plant Cell*, **20**, 1278–1288.

Zhou, L., Gao, G., Tang, R., Wang, W., Wang, Y., Tian, S. et al. (2022) M^6 A-mediated regulation of crop development and stress responses. *Plant Biotechnology Journal*, **20**, 1447–1455.